

# Optimal Sliding Correlator Channel Sounder Design

Ryan J. Pirkl, *Student Member, IEEE*, and Gregory D. Durgin, *Senior Member, IEEE*

**Abstract**—The sliding correlator technique remains one of the most versatile and effective methods for sounding the radio propagation channel in next-generation wireless systems. Despite their utility, there has never been a comprehensive set of metrics and rules for the design of a sliding correlator channel sounder. This paper presents quantitative guidelines for balancing the many system parameters to achieve optimal levels of temporal resolution, dynamic range, processing gain, and Doppler resolution. The design procedure presented at the end of the paper will allow researchers to probe the new radioscaples that result as wireless systems are pushed to higher carrier frequencies, wider bandwidths, multiple antennas, and ubiquitous operation.

**Index Terms**—Swept time-delay, sliding correlator, spread spectrum, channel sounder design, wireless channel measurements.

## I. INTRODUCTION

THE UTILITY and simplicity of the sliding correlator channel sounder has made it the indispensable tape measure in the tool belt of radio propagation engineers [1]–[4]. First used by Cox in [5], the sliding correlator technique provides a cost-effective method for sounding the ever-growing bandwidths of next-generation wireless channels. Unlike the network analyzer, which can be a prohibitively expensive single-box solution, the sliding correlator channel sounder may be constructed from off-the-shelf components at relatively little cost while affording the advantage of a physically separable transmitter and receiver. Tether-free operation allows for measurements of indoor, outdoor, and mobile radio channels but can complicate the extraction of absolute delay and phase information. However, whereas both network analyzers and impulse-based channel sounders are susceptible to interferences, the sliding correlator approach is inherently robust through the use of direct sequence spread spectrum (DSSS) signals [6]. DSSS also provides improved measurement dynamic range and low peak-power levels, which allow the channel sounder to perform non-invasive measurements of interference-sensitive channels [7]. Additionally, the sliding correlator provides the distinct advantage of bandwidth compression through temporal dilation, making it an ideal approach for measuring the huge bandwidths of the ultra-wideband channel [8], [9]. It should be noted that the chirp-based channel sounder offers similar wideband channel characterization with bandwidth compression [10]. However, the architecture remains considerably less popular, likely due to its greater system complexity as well

as the difficulties inherent in implementing floating point gate arrays and direct frequency synthesizers [11].

Despite its pervasiveness, the details of designing an optimal sliding correlator channel sounder remain unclear. System design commonly employs a combination of rule-of-thumb and guess-and-test methods that rely on erroneous approximations of the realized system's dynamic range and necessitate tedious tweaking to attain expected performance levels [12]. Optimizing the design process, however, requires accurate quantitative descriptions of the channel sounder's capabilities. The first rigorous mathematical treatment of the sliding correlator was given by Benvenuto [13]. Talvitie et al. expanded upon this analysis by qualitatively describing the relationships between the sliding correlator's design parameters and its dynamic range [14]. Martin used numerical simulations to generate plots of dynamic range versus slide factor for various pseudo-random noise (PN) lengths and included a systematic design methodology based on these plots [15].

The work contained herein unifies and expands upon these prior contributions, offering a *complete* picture of the sliding correlator channel sounder's operation based upon a detailed analysis of the system's dynamic range. Through this analysis, we develop: 1) an *optimal* slide factor, 2) a *realistic* expression for the system's dynamic range, 3) a systematic design methodology, and 4) a spectral interpretation of the system's time-varying channel measurement. Discussion begins with a review of pseudo-random noise and its role in wireless channel sounding. We then introduce the sliding correlator technique and provide a rigorous analysis of its operation. Based upon this analysis, we develop a set of design equations for the sliding correlator channel sounder and present an optimal design methodology. Finally, we address practical considerations for design and measurement including how the system is affected by time-varying channels.

## II. PSEUDO-RANDOM NOISE FOR CHANNEL SOUNDING

The time-domain channel sounder requires a predetermined signal such that the exact transmitted signal is known at the receiver a priori. The ideal signal statistics would resemble those of Gaussian white noise, which may be approximated by pseudo-random noise. The noise-like properties of pseudo-random noise stem from its corresponding pseudo-random binary sequence.

### A. Pseudo-Random Binary Sequences

Consider a *pseudo-random binary sequence*  $a_i$  where  $a_i \in \{0, 1\}$ .  $a_i$  is a finite repeating sequence with a period  $L$  such that  $a_{i+L} = a_i$ . One method of generating such a sequence is through a recursive algorithm whereby the  $n^{th}$  term in

Manuscript received March 16, 2007; revised April 23, 2008; accepted July 3, 2008. The associate editor coordinating the review of this paper and approving it for publication was K. Sowerby. This work was supported by the National Science Foundation Graduate Research Fellowship.

The authors are with the Propagation Group in the School of Electrical and Computer Engineering, Georgia Institute of Technology (e-mail: rpirkl@gatech.edu, durgin@ece.gatech.edu).

Digital Object Identifier 10.1109/TWC.2008.070278.

the sequence is determined from a linear combination of the previous  $N$  terms.

$$a_n = \sum_{i=1}^N c_i a_{n-i} \quad (1)$$

In (1),  $c_i \in \{0,1\}$  are the feedback coefficients that determine which of the previous  $N$  terms contribute to the value of the  $n^{\text{th}}$  term. Note that to determine the zeroth term in the sequence, one requires knowledge of  $\{a_{-N}, a_{1-N}, \dots, a_{-2}, a_{-1}\}$ . It is assumed that  $c_N = 1$  so that  $a_{n-N}$  is required to calculate  $a_n$ . Further, it should be noted that the operators described in (1) involve Boolean arithmetic (i.e., the summation uses modulo 2 addition).

Using the feedback coefficients  $c_i$ , one may describe  $a_i$  by a *characteristic polynomial*  $f(x)$  according to

$$f(x) = 1 - \sum_{i=1}^N c_i x^i \quad (2)$$

Let us define a polynomial  $G(x)$  as the reciprocal of  $f(x)$ .

$$G(x) = \frac{1}{f(x)} \quad (3)$$

It can be shown that the coefficients of the terms of  $G(x)$  are themselves the terms from the pseudo-random binary sequence  $a_i$ . Therefore,  $G(x)$  is commonly referred to as the *generating function* of  $a_i$  [16].

$$G(x) = \sum_{i=0}^{\infty} a_i x^i \quad (4)$$

One important caveat of Equation (4) is that it assumes the sequence as derived from Equation (1) was seeded such that  $\{a_{-N}, a_{1-N}, \dots, a_{-2}\} = 0$  and  $\{a_{-1}\} = 1$ . For any other seeding such that the  $N$  initial terms are not all simultaneously zero, the resulting pseudo-random binary sequence will be a phase shifted version of  $a_i$  in (4).

### B. Maximal Sequences

An important class of pseudo-random binary sequences are *maximal sequences*, or *m-sequences* for short. M-sequences have the longest possible period  $L$  for a sequence produced from the recursive algorithm in (1) that uses the previous  $N$  terms [6]. The period of an m-sequence is given by

$$L = 2^N - 1 \quad (5)$$

Therefore, the most “efficient” characteristic polynomials will produce m-sequences, as they lead to the longest non-repeating sequences from the fewest previous terms. All discussions of pseudo-random binary sequences henceforth will imply m-sequences.

### C. Linear Feedback Shift Register

The *linear feedback shift register* (LFSR) is a hardware realization of the recursive algorithm described by Equation (1). An  $N$ -bit shift register holds the previous  $N$  terms of the m-sequence. To determine  $a_n$ , the terms in the  $i^{\text{th}}$  registers are weighted according to their respective feedback coefficients  $c_i$  and summed modulus 2 using XOR gates. At each clock cycle,

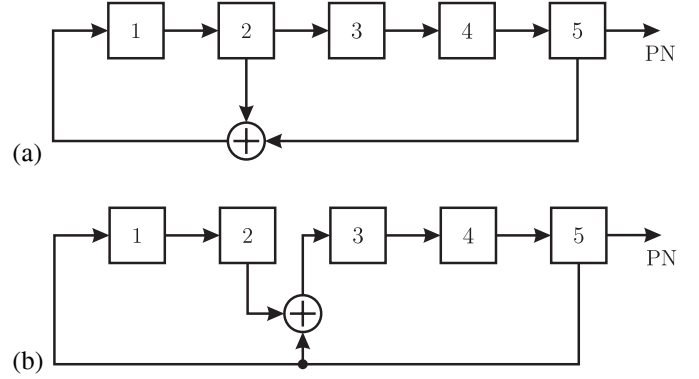


Fig. 1. Examples of the two linear feedback shift register architectures: (a) simple shift register generator (SSRG) and (b) modular shift register generator (MSRG). The  $\oplus$  denotes modulo 2 addition.

the summation is fed into the input of the shift register and the  $(n - N)^{\text{th}}$  term is shifted out. This implementation is known as the *simple shift register generator* (SSRG) and is depicted in Figure 1(a) [6]. Only registers corresponding to  $c_i = 1$  are used as part of the feedback configuration. Thereby, the set of feedback registers,  $F_s$ , for the SSRG architecture may be determined according to

$$F_s = \{i\} \text{ for all } i > 0 \text{ such that } c_i = 1 \quad (6)$$

The characteristic polynomial  $f(x)$  described in (2) may be recognized as an exact description of the feedback configuration of the SSRG. For example, if the characteristic polynomial was  $f(x) = 1 - x^2 - x^5$ , then when  $i = \{2, 5\}$ ,  $c_i = 1$ . Therefore, the set of feedback registers is  $F_s = \{2, 5\}$ .

Figure 1(b) shows an alternative implementation of the linear feedback shift register called the *modular shift register generator* (MSRG) [6]. Whereas the SSRG feedback configuration involves multiple register outputs and a single shift register input, the MSRG feedback configuration involves a single register output and multiple register inputs. In the MSRG architecture, the output of the  $N^{\text{th}}$  register is summed modulus 2 with the output of the  $(j - 1)^{\text{th}}$  register and fed into the  $j^{\text{th}}$  register. The output of the  $N^{\text{th}}$  register also feeds the input of the shift register. Note that for the MSRG, the characteristic polynomial does not directly describe the feedback configuration. The set of feedback registers in the MSRG architecture, denoted  $F_m$ , may be determined according to

$$F_m = \{j, N\} \quad (7)$$

where

$$j = N - i \text{ for all } i < N \text{ such that } c_i = 1 \quad (8)$$

For example, if the characteristic polynomial was  $f(x) = 1 - x^2 - x^5$ , then when  $i = \{2, 5\}$ ,  $c_i = 1$ . Noting that  $N = 5$ , we have  $j = \{3\}$  and  $F_m = \{3, 5\}$ .

The SSRG architecture is generally simpler to implement but can suffer from long propagation delays through the cascade of XOR gates. The MSRG architecture provides a very flexible template should one wish to create a reconfigurable pseudo-random binary sequence generator. Also, the parallel arrangement of the XOR gates provides shorter propagation delays along the feedback loop, thereby allowing faster clock

rates. However, the tradeoff is the added complexity of the design.

#### D. Analog Representation

Consider an  $N$ -bit linear feedback shift register configured as a simple shift register generator. The feedback registers  $F_s$  are selected such that the resulting pseudo-random binary sequence  $a_i$  is an m-sequence of length  $L = 2^N - 1$ . The shift register is clocked at a frequency of  $f_c$  such that, after every  $1/f_c$  seconds, the next term of the m-sequence is generated. Each term of the m-sequence will be represented by a rectangular pulse with duration  $T_c = 1/f_c$ . Let us assume a biphasic output with amplitude  $\pm V_0$  whereby  $a_i = 0$  corresponds to  $-V_0$  and  $a_i = 1$  corresponds to  $+V_0$ . This arrangement produces an analog waveform  $x(t)$  that is the *pseudo-random noise* (PN) derived from the m-sequence  $a_i$ . We may represent  $x(t)$  as

$$x(t) = \sum_{i \in \mathbb{Z}} V_0(2a_i - 1)\Pi(t/T_c - i - 1/2) \quad (9)$$

where  $\mathbb{Z}$  is the set of all real integers,  $\Pi(\xi)$  is the rectangular function given by

$$\Pi(\xi) = u(1/2 - |\xi|) \quad (10)$$

and  $u(\xi)$  is the Heaviside step function. Thus, the PN is an infinite train of rectangular pulses with the value of the  $i^{\text{th}}$  pulse determined by the  $i^{\text{th}}$  term of the m-sequence. It is common to refer to each pulse as a *chip*. Similarly, the shift register clock rate  $f_c$  is commonly referred to as the *chip rate* [17].

#### E. PN Autocorrelation

The autocorrelation of the PN in Equation (9) is

$$C_x(\tau) = V_0^2 \left[ \sum_{i \in \mathbb{Z}} \left\{ (1 + 1/L) \Lambda\left(\frac{\tau - iLT_c}{T_c}\right) \right\} - \frac{1}{L} \right] \quad (11)$$

where  $\Lambda(\xi)$  is the triangle function given by

$$\Lambda(\xi) = (1 - |\xi|)u(1 - |\xi|) \quad (12)$$

Equation (11) describes a train of triangular pulses with a base width of  $2T_c$ , a maximum amplitude of  $V_0^2$ , a period of  $LT_c$ , and a DC offset of  $-V_0^2/L$  [13].

#### F. PN Frequency Spectrum

Using Fourier analysis, the PN spectrum,  $\tilde{X}(f)$ , is found to be

$$\tilde{X}(f) = \frac{V_0}{L} \sum_{k \in \mathbb{Z}} \text{sinc}\left(\frac{k}{L}\right) \delta\left(f - \frac{f_c k}{L}\right) e^{j \frac{k\pi}{L}} \times \sum_{i=1}^L \left[ (2a_i - 1) e^{-j \frac{k2\pi}{L} i} \right] \quad (13)$$

where  $\delta(\xi)$  is the Dirac delta function and  $\text{sinc}(x) = (\sin \pi * x)/(\pi * x)$ . Thus, the spectrum of a PN is shown to be a train of Dirac delta functions at integer multiples of  $f_c/L$ . The magnitude of the spectrum is bounded by  $\text{sinc}(k/L)$ . Figure 2 shows the magnitude of the spectrum of a PN derived from an m-sequence of length  $L = 31$ . Note that the majority of the power is concentrated between  $f_c$  and  $-f_c$ .

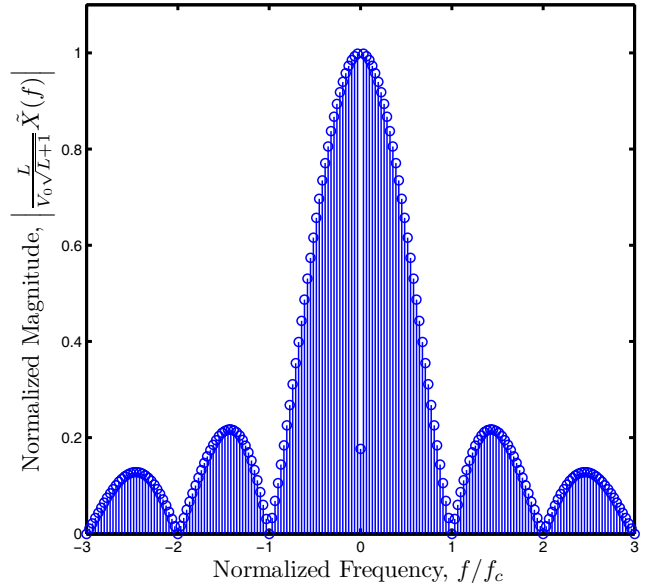


Fig. 2. The frequency spectrum of a PN is characterized by a train of Dirac delta functions under a  $\text{sinc}(f/f_c)$  envelope.

### III. SPREAD SPECTRUM CHANNEL SOUNDING

The PN is the noise-like signal that will be transmitted through the wireless channel. At the receiver, we might detect the presence of the originally transmitted signal by means of cross-correlation with the received signal similar to a correlation receiver. For two signals  $\xi(t)$  and  $\zeta(t)$ , the cross-correlation  $C_{\xi\zeta}(\tau)$  is given by

$$C_{\xi\zeta}(\tau) = \int_{-\infty}^{\infty} \xi(t) \zeta^*(t - \tau) dt \quad (14)$$

where  $(\cdot)^*$  is the complex conjugate of  $(\cdot)$ .

Let us assume a fixed, static wireless channel, which we shall model as a tapped-delay line whereby individual multipath components are delayed and complex-scaled copies of the transmitted signal [18]. The channel impulse response (CIR)  $\tilde{H}(\tau)$  may be expressed as the summation of  $N$  Dirac delta functions, each with a complex amplitude  $\tilde{\alpha}_i$  and delay  $\tau_i$ .

$$\tilde{H}(\tau) = \sum_{i=1}^N \tilde{\alpha}_i \delta(\tau - \tau_i) \quad (15)$$

If the PN  $x(t)$  were transmitted through the wireless channel described by  $\tilde{H}(\tau)$ , the received signal  $\tilde{y}(t)$  will be a train of delayed and attenuated copies according to

$$\tilde{y}(t) = \sum_{i=1}^N \tilde{\alpha}_i x(t - \tau_i) \quad (16)$$

We find that the cross-correlation  $C_{x\tilde{y}}(\tau)$  is then

$$C_{x\tilde{y}}(\tau) = \sum_{i=1}^N \tilde{\alpha}_i C_x(\tau - \tau_i) \quad (17)$$

where  $C_x(\tau)$  is the autocorrelation of  $x(t)$  described in (11). Note that (17) is equivalently the tapped-delay line representation of the wireless channel convolved with the autocorrelation

of the transmitted signal. Thus,  $C_{x\tilde{y}}(\tau)$  is equivalently a scaled copy of the band-limited CIR,  $\tilde{H}_{BL}(\tau)$ , as measured using  $x(t)$ .

$$\tilde{H}_{BL}(\tau) = \frac{1}{V_0^2} C_{x\tilde{y}}(\tau) \quad (18)$$

This is the direct result of a spread spectrum channel sounder such as that used in [19].

#### A. Practical Considerations

The cross-correlation described in Equation (17) is typically implemented in software. The received signal  $\tilde{y}(t)$  would be sampled by an analog-to-digital converter (ADC), and the data would either be processed by an FPGA or stored on a computer for post-processing. To properly digitize the received signal, the ADC's sampling rate must be equal to or greater than twice the baseband bandwidth. For narrow-band measurements, this issue is rather trivial. However, as the measurement bandwidth increases, so too does the cost of the required high-speed ADC. Thus, to ease the hardware requirements for measuring wideband wireless channels, researchers have used the sliding correlator technique described in [5] to time-dilate the channel impulse response.

### IV. SLIDING CORRELATOR

The purpose of the sliding correlator is to produce a time-dilated PN autocorrelation, which will lead to a time-dilated cross-correlation according to (17). Whereas the true autocorrelation uses two *identical* signals, the sliding correlator's autocorrelation involves two *similar* signals, whereby one signal is clocked at a slightly slower rate compared to the other. Multiplying these two similar signals together and carefully filtering their product will yield a very close approximation to a time-dilated autocorrelation.

#### A. Multiplying the PNs

Consider two PNs  $x(t)$  and  $x'(t)$  with chip rates  $f_c$  and  $f'_c$  respectively. The PNs are derived from the same m-sequence of length  $L$  and have identical amplitudes such that  $V_0 = V'_0$ . Now, consider the waveform  $p(\tau)$ , which we shall call the *sliding correlator product* of the two PNs.

$$p(\tau) = x(\tau)x'(\tau) \quad (19)$$

Multiplication in the time domain is equivalently convolution in the frequency domain. Defining  $\tilde{P}(f)$ ,  $\tilde{X}(f)$ , and  $\tilde{X}'(f)$  as the Fourier transform pairs of  $p(\tau)$ ,  $x(\tau)$ , and  $x'(\tau)$ , respectively, Equation (19) is equivalently

$$\tilde{P}(f) = \tilde{X}(f) \otimes \tilde{X}'(f) \quad (20)$$

For the PN spectrum described in (13), the convolution of two PN spectrums with chip rates  $f_c$  and  $f'_c$  is

$$\begin{aligned} \tilde{P}(f) = & \left( \frac{V_0}{L} \right)^2 \sum_{k, k' \in \mathbb{Z}} \left\{ \delta \left( f - \frac{f_c k + f'_c k'}{L} \right) \times \right. \\ & \left. \text{sinc} \left( \frac{k}{L} \right) \text{sinc} \left( \frac{k'}{L} \right) e^{-j \frac{\pi}{T} (k+k')} \times \right. \\ & \left. \sum_{i=1}^L \sum_{i'=1}^L \left[ (2a_i - 1) (2a_{i'} - 1) e^{-j \frac{\pi}{T} (ki+k'i')} \right] \right\} \quad (21) \end{aligned}$$

Close inspection of (21) reveals that when  $k' = -k$ ,  $\tilde{P}(f)$  collapses into the spectrum corresponding to a train of triangle-shaped pulses, which we will here denote as  $\tilde{Q}_c(f)$ .

$$\begin{aligned} \tilde{Q}_c(f) = & \left( \frac{V_0}{L} \right)^2 \sum_{k \in \mathbb{Z}} \left\{ \delta \left( f - k \frac{f_c - f'_c}{L} \right) \text{sinc}^2 \left( \frac{k}{L} \right) \times \right. \\ & \left. \sum_{i=1}^L \sum_{i'=1}^L \left[ (2a_i - 1) (2a_{i'} - 1) e^{-j \frac{\pi}{T} k(i-i')} \right] \right\} \quad (22) \end{aligned}$$

Equation (22) is the spectrum of the time-dilated autocorrelation [13]. The remaining terms in the double summation of (21) represent the distortion to the time-dilated autocorrelation due to the sliding correlation. The frequency-domain distortion is here denoted as  $\tilde{Q}_d(f)$ .

$$\begin{aligned} \tilde{Q}_d(f) = & \left( \frac{V_0}{L} \right)^2 \sum_{\substack{k, k' \in \mathbb{Z} \\ k' \neq -k}} \left\{ \delta \left( f - \frac{f_c k + f'_c k'}{L} \right) \times \right. \\ & \left. \text{sinc} \left( \frac{k}{L} \right) \text{sinc} \left( \frac{k'}{L} \right) e^{-j \frac{\pi}{T} (k+k')} \times \right. \\ & \left. \sum_{i=1}^L \sum_{i'=1}^L \left[ (2a_i - 1) (2a_{i'} - 1) e^{-j \frac{\pi}{T} (ki+k'i')} \right] \right\} \quad (23) \end{aligned}$$

Let  $q_c(\tau)$  and  $q_d(\tau)$  represent the inverse Fourier transform for  $\tilde{Q}_c(f)$  and  $\tilde{Q}_d(f)$  respectively. The sliding correlator product,  $p(\tau)$ , may then be expressed as the superposition of the autocorrelation signal  $q_c(\tau)$  and the distortion signal,  $q_d(\tau)$  as discussed in [13].

$$p(\tau) = q_c(\tau) + q_d(\tau) \quad (24)$$

Figure 3(a) compares the spectrum for the time-dilated autocorrelation spectrum  $\tilde{Q}_c(f)$  with its accompanying distortion spectrum  $\tilde{Q}_d(f)$  for the case of  $L = 31$  and  $f'_c = 0.99f_c$ . Figure 3(b) compares the corresponding time-domain signals  $q_c(\tau)$  and  $q_d(\tau)$  for the same scenario. The time-dilated autocorrelation can be clearly seen in Figure 3(b). However, it is also apparent that the magnitude of the distortion signal  $q_d(\tau)$  is comparable to that of the time-dilated autocorrelation signal  $q_c(\tau)$ . Therefore, it is important that one remove this distortion to produce a "clean" time-dilated autocorrelation.

#### B. Slide Factor

It is convenient to define the *slide factor*,  $\gamma$ , as the ratio of  $f_c$  to the difference between  $f_c$  and  $f'_c$  [5].

$$\gamma = \frac{f_c}{f_c - f'_c} \quad (25)$$

The slide factor may be perceived as the temporal dilation factor for the sliding correlator's time-dilated autocorrelation. Therefore,  $q_c(\tau)$  may be equivalently expressed as

$$q_c(\tau) = C_x \left( \frac{\tau}{\gamma} \right) \quad (26)$$

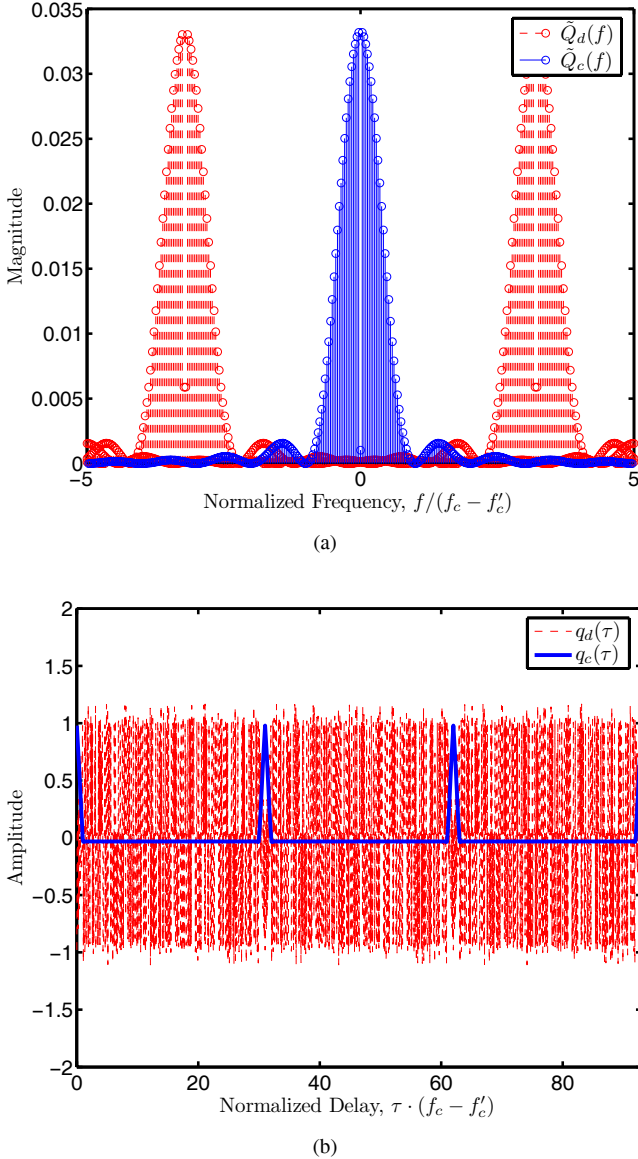


Fig. 3. A comparison of the sliding correlator's autocorrelation and distortion signals for  $L = 31$  and  $f'_c = 0.99f_c$ : (a) frequency domain and (b) time domain.

### C. Filtering the Product

The simplest means of removing the unwanted distortion introduced by  $q_d(\tau)$  is by low-pass filtering the sliding correlator product  $p(\tau)$ . The time-dilated autocorrelation's spectrum  $\tilde{Q}_c(f)$  is centered at DC and has a  $\text{sinc}^2(f\gamma/f_c)$  envelope. Thus, the majority of its power resides within the main lobe as bounded by  $f \in (-|f_c/\gamma|, |f_c/\gamma|)$ . Let us assume an ideal rectangular low-pass filter,  $\tilde{h}(f)$  with impulse response,  $H(\tau)$ , such that

$$\tilde{h}(f) = \mathbf{u}(f + |f_c/\gamma|) - \mathbf{u}(f - |f_c/\gamma|) \quad (27)$$

By filtering  $p(\tau)$  with  $H(\tau)$ , a significant portion of the unwanted distortion will be removed while passing the majority of the time-dilated autocorrelation. However, filtering is only part of the solution for removing  $q_d(\tau)$ . The optimal approach requires the concerted selection of  $\gamma$  and  $L$  so that the majority of the distortion signal's power will be blocked by the low-pass filter.

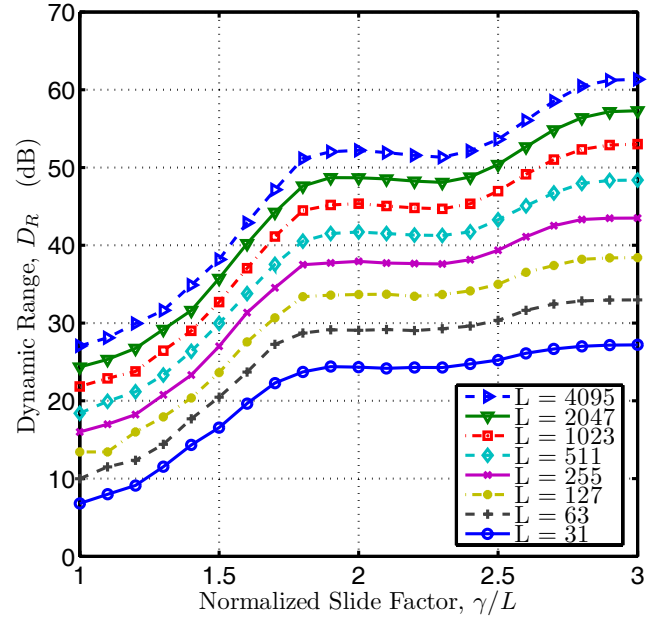


Fig. 4. A comparison of the average  $D_R$  for sets of four PN's with  $L = \{31, 63, 127, 511, 1023, 2047, 4095\}$ .

### D. Optimization

To produce a “clean” time-dilated autocorrelation, we must minimize the amplitude of the distortion signal  $q_d(\tau)$ . Here it is useful to define the measurement dynamic range  $D_R$  of a sliding correlator in dB as

$$D_R = 20 \log_{10} \left( \frac{\max(|Lq_c(\tau) \otimes H(\tau)|)}{\max(|Lq_d(\tau) \otimes H(\tau) - V_0^2|)} \right) \quad (\text{dB}) \quad (28)$$

For the ideal case of no distortion, we might remove the low-pass filter by setting  $H(\tau)$  to  $\delta(\tau)$ . The dynamic range would then be  $D_{R,ideal}$  as defined in Equation (29).

$$D_{R,ideal} = 20 \log_{10}(L) \quad (\text{dB}) \quad (29)$$

Equation (29) is the typical result for a DSSS system using a true correlation receiver [6]. The distortion signal produced by the sliding correlator leads to a reduction in the dynamic range. Mathematically describing this degradation in dynamic range is difficult due to the nonlinear  $\max(\cdot)$  operation on the complicated distortion signal described by (23). However, simulations based on Equation (28) indicate interesting trends for  $D_R$  with increasing slide factors. Figure 4 compares the dynamic range of PN's of various lengths for a range of  $\gamma/L$  values. For the simulation, the PN spectrums  $\tilde{X}(f)$  and  $\tilde{X}'(f)$  were restricted to the range  $f \in [-3f_c, 3f_c]$  and  $f \in [-3f'_c, 3f'_c]$ , respectively to minimize both memory requirements and processing time. The dynamic range  $D_R$  was calculated using (28).

For a given PN of length  $L$ , Figure 4 indicates an increase in  $D_R$  for increasing  $\gamma/L$  with local maxima occurring near integer multiples of  $\gamma/L$ .  $\gamma/L = 2$  seems to be a particularly critical point for the dynamic range. For small  $L$ , increasing the slide factor beyond  $2L$  provides only a small improvement in the dynamic range. However, for large  $L$ , the increase in dynamic range becomes more substantial for increased  $\gamma$  values.

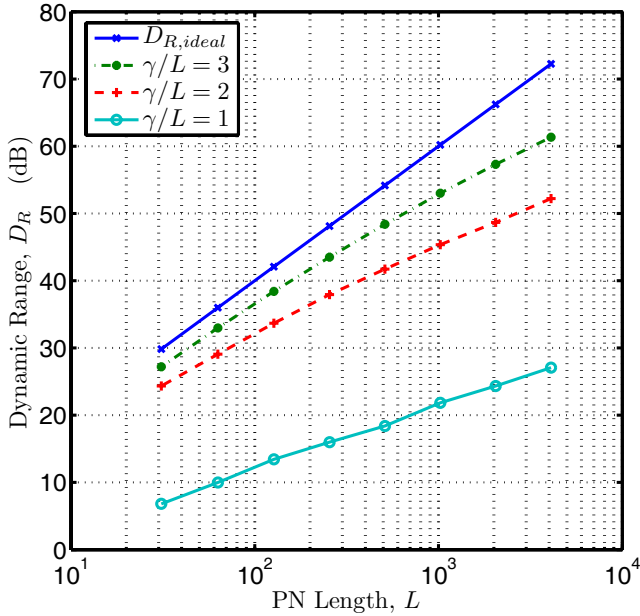


Fig. 5. A comparison of  $D_{R,ideal}$  to the dynamic range of PNs with  $\gamma/L = \{1, 2, 3\}$  for a range of PN lengths  $L$ .

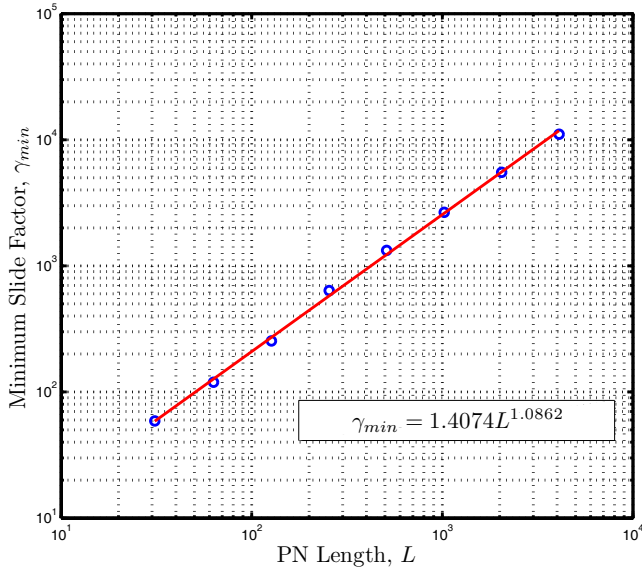


Fig. 6. Linear regression performed on the points corresponding to the slide factor for a given PN length that achieves a dynamic range within 20% of ideal.

This is made more evident by Figure 5, which plots dynamic range as a function of  $L$  for select  $\gamma/L$  values. The uppermost trace is  $D_{R,ideal}$  as given by (29). For all PN lengths, there is a marked improvement in dynamic range when  $\gamma/L$  is increased from 1 to 2. For small  $L$ , this appears to bring the dynamic range fairly close to  $D_{R,ideal}$ . However, for large  $L$ , the dynamic range will fall well below ideal. Specifically, when  $L \leq 63$ , using the  $\gamma/L = 2$  rule-of-thumb will yield a dynamic range that is approximately  $0.8D_{R,ideal}$ . However, for  $L > 63$  and  $\gamma/L = 2$ ,  $D_{R,ideal}$  becomes an increasingly poor approximation for the sliding correlator's dynamic range. When  $L = 4095$  and  $\gamma/L = 2$ , the  $D_{R,ideal}$  approximation errs by over 27%.

Using the simulations results, an empirical formula was derived for  $\gamma_{min}$ , which is the minimum slide factor that provides a dynamic range within 20% of the ideal. Figure 6 plots the slide factor associated with a particular PN length that produces a dynamic range  $D_R = 0.8D_{R,ideal}$ . Linear regression analysis on the log-log plot leads to the following empirical equation for  $\gamma_{min}$ .

$$\gamma_{min} = 1.41L^{1.09} \quad (30)$$

For any  $\gamma \geq \gamma_{min}$ , the dynamic range of the sliding correlator will be in the range  $0.8D_{R,ideal} \leq D_R < D_{R,ideal}$  (dB). Thus, we may safely approximate the dynamic range as being equal to the lower bound of  $0.8D_{R,ideal}$ .

$$D_R \approx 16 \log_{10}(L) \text{ (dB) for } \gamma \geq \gamma_{min} \quad (31)$$

### E. Time-Dilated Autocorrelation Approximation

Before filtering, the sliding correlator product  $p(\tau)$  is the superposition of two signals:  $q_c(\tau)$  and  $q_d(\tau)$ . Let us set  $\gamma$  to  $\gamma_{min}$  and filter  $p(\tau)$  with the ideal rectangular low-pass filter  $H(\tau)$  described earlier. The result will be the sliding correlator's approximation to the time-dilated PN autocorrelation.

$$C_{x,sc}(\tau) = p(\tau) \otimes H(\tau) \quad (32)$$

Substituting (24) and distributing the convolution operator, we find

$$C_{x,sc}(\tau) = q_c(\tau) \otimes H(\tau) + q_d(\tau) \otimes H(\tau) \quad (33)$$

Recall that  $H(\tau)$  was constructed to pass the main lobe of  $\hat{Q}_c(f)$ . Thus, we shall make the following approximation:

$$q_c(\tau) \otimes H(\tau) \approx q_c(\tau) \quad (34)$$

Additionally, we selected  $\gamma$  in concert with  $L$  to minimize the distortion signal and maximize the dynamic range. Thus, we shall make one additional approximation.

$$q_d(\tau) \otimes H(\tau) \approx 0 \quad (35)$$

Using these approximations as well as the relationship defined in (26), we find that (32) simplifies to

$$C_{x,sc}(\tau) \approx C_x\left(\frac{\tau}{\gamma}\right) \quad (36)$$

Figure 7 examines the approximation made in (36). Excepting for a 10% decrease in peak amplitude, the traces are nearly identical, indicating that the approximation is valid. Therefore, with careful selection of  $\gamma$  relative to  $L$ , the output of a sliding correlator will approximate a time-dilated PN autocorrelation.

## V. SLIDING CORRELATOR CHANNEL SOUNDING

Let us now consider the CIR of a fixed static wireless channel as measured by a sliding correlator channel sounder. We will assume the actual CIR,  $\tilde{H}(\tau)$ , fits the tapped-delay line model described by Equation (15). Our transmitted signal  $x(t)$  is a PN of length  $L$  with a chip rate  $f_c$  as described in (9). At the receiver, the received signal  $\tilde{y}(t)$  is processed via sliding correlation; that is, it is multiplied by  $x'(t)$ , which is a PN derived from the same m-sequence as  $x(t)$  but with a chip rate  $f'_c$  where  $f'_c < f_c$ . Let us choose  $f_c$  and  $f'_c$  such that  $\gamma = \gamma_{min}$  and filter the output of the sliding

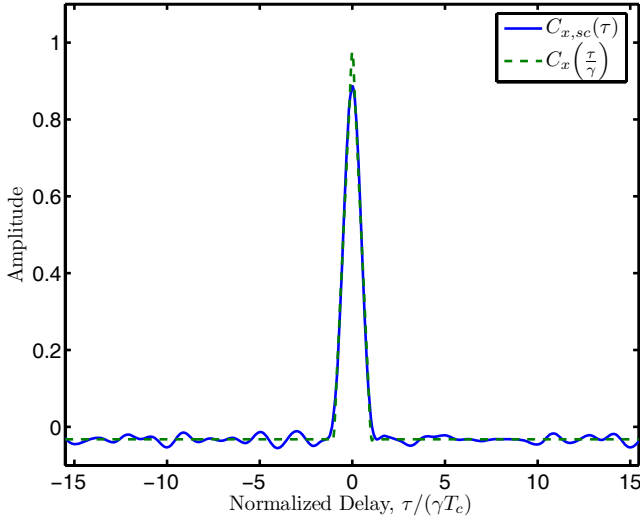


Fig. 7. A comparison of the sliding correlator output,  $C_{x,sc}(\tau)$ , versus a time-dilated version of the PN autocorrelation given by  $C_x(\tau/\gamma)$ .

correlator with the ideal low-pass filter  $H(\tau)$  described by  $\tilde{h}(f)$  in (27). Analogous to the sliding correlator's time-dilated autocorrelation described in (36), the filtered output of a sliding correlator channel sounder will approximate a time-dilated cross-correlation, denoted  $C_{x\tilde{y},sc}(\tau)$ .

$$C_{x\tilde{y},sc}(\tau) \approx C_{x\tilde{y}}\left(\frac{\tau}{\gamma}\right) \quad (37)$$

Equation (37) implies that  $C_{x\tilde{y},sc}(\tau)$  is the same band-limited CIR as described by  $C_{x\tilde{y}}(\tau)$ , albeit time-dilated. This is a powerful statement, so let us examine it more carefully. Substituting (17) for  $C_{x\tilde{y}}(\tau)$ , we have

$$C_{x\tilde{y},sc}(\tau) \approx \sum_{i=1}^N \tilde{\alpha}_i C_x\left(\frac{\tau}{\gamma} - \tau_i\right) \quad (38)$$

Rearranging terms and making use of (36) yields

$$C_{x\tilde{y},sc}(\tau) = \sum_{i=1}^N \tilde{\alpha}_i C_{x,sc}(\tau - \gamma\tau_i) \quad (39)$$

Note that although (37) was an approximation, (39) is exact. Substituting (32) for  $C_{x,sc}(\tau)$ , we arrive at an exact equation for  $C_{x\tilde{y},sc}(\tau)$ .

$$C_{x\tilde{y},sc}(\tau) = \sum_{i=1}^N \tilde{\alpha}_i [p(\tau - \gamma\tau_i) \otimes H(\tau)] \quad (40)$$

Figure 8 compares  $C_{x\tilde{y},sc}(\tau)$  as approximated in Equation (37) with the exact formulation described by Equation (40). The nearly identical shape of the traces leads us to conclude that the approximation for  $C_{x\tilde{y},sc}(\tau)$  made in (37) is valid. Therefore, by reversing the time-dilation and scaling the signal, we may “undo” the effects of the sliding correlator and obtain a close approximation to the  $\tilde{H}_{BL}(\tau)$  described in Equation (18).

$$\tilde{H}_{BL}(\tau) \approx \frac{1}{V_0^2} C_{x\tilde{y},sc}(\gamma\tau) \quad (41)$$

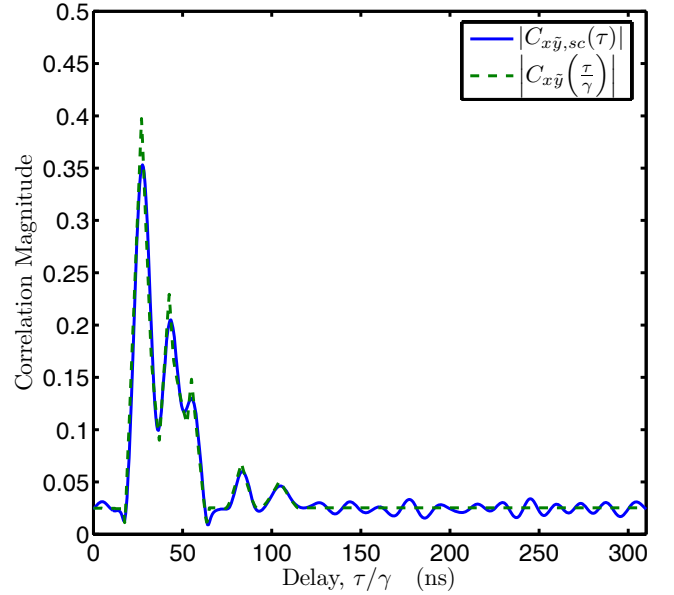


Fig. 8. A comparison of the sliding correlator channel sounder's output,  $C_{x\tilde{y},sc}(\tau)$ , versus a time-dilated version of the wireless channel cross-correlation given by  $C_{x\tilde{y}}(\tau/\gamma)$  for an arbitrary  $\tilde{H}(\tau)$ .

TABLE I  
SLIDING CORRELATOR CHANNEL SOUNDER DESIGN EQUATIONS

Capability	Equation	Dependencies
Doppler Resolution	$f_{D,max} = \frac{f_c}{2\gamma L}$	$f_c, \gamma, L$
Processing Gain	$G_p = 10 \log_{10}(\gamma)$ (dB)	$\gamma$
Dynamic Range	$D_R \approx 16 \log_{10}(L)$ (dB)	$\gamma \geq 1.41L^{1.09}, L$
Temporal Resolution	$T_{res} = \frac{1}{f_c}$	$f_c$
Maximum Multipath Delay	$\tau_{max} = \frac{L}{f_c}$	$f_c, L$
Maximum Path Length	$d_{max} = c \frac{L}{f_c}$	$f_c, L$

Equation (41) is therefore the approximation to the band-limited CIR that one would obtain if measuring the wireless channel using a sliding correlator channel sounder.

## VI. CHANNEL SOUNDER CAPABILITIES

The fidelity of the band-limited CIR produced by the sliding correlator channel sounder is dependent on the system capabilities, which are themselves dependent on just three system parameters: the transmitter PN chip rate  $f_c$ , the PN length  $L$ , and the slide factor  $\gamma$ . Table I summarizes the channel sounder's capabilities and the parameters that affect them.

### A. Doppler Resolution

The Doppler resolution is the largest Doppler frequency that can be measured unambiguously with the sliding correlator channel sounder. The channel sounder records a measurement

of the CIR once every  $\gamma L/f_c$  seconds. Therefore, the channel sounder's Doppler resolution is given by

$$f_{D,max} = \frac{f_c}{2\gamma L} \quad (42)$$

### B. Processing Gain

The processing gain is defined as the ratio of the SNR after a process to the SNR before the process [6]. Thus, in dB, processing gain,  $G_p$ , is

$$G_p = 10 \log_{10} \left( \frac{SNR_{out}}{SNR_{in}} \right) \quad (\text{dB}) \quad (43)$$

Processing gain acts to spread the power spectrum of unwanted noise and interferents. Consider a DC offset that is the complex-baseband equivalent of a continuous wave interferent at the system's RF carrier. Multiplication with the receiver PN,  $x'(t)$ , will spread the interferent's power spectral density across a complex-baseband bandwidth of approximately  $f'_c$ . Filtering with the ideal low-pass filter will block the interferent's spread spectrum at frequencies above  $f_c - f'_c$  such that only  $100 \times (f_c - f'_c)/f'_c\%$  of the interferent's power will remain. Assuming  $f'_c \approx f_c$ , the interferent's power will be reduced by a factor of  $\gamma$ . Thus, the linear processing gain for a sliding correlator system is simply  $\gamma$ , which in dB is

$$G_p = 10 \log_{10}(\gamma) \quad (\text{dB}) \quad (44)$$

Note that (44) differs from a direct sequence spread spectrum system's processing gain, which may be approximated by  $10 \log_{10}(L)$  [6]. This is due to the sliding correlator operation.

### C. Dynamic Range

The dynamic range of a sliding correlator was discussed in detail in Section IV-D. In summary, by establishing an empirical formula for the minimum slide factor,  $\gamma_{min}$ , we were able to approximate the dynamic range according to the lower bound presented in Eq. (31).

### D. Temporal Resolution

The temporal resolution defines how precisely one may resolve the relative delay of a given multipath component. For a sliding correlator channel sounder, the temporal resolution  $T_{res}$  is estimated as

$$T_{res} = \frac{1}{f_c} \quad (45)$$

### E. Maximum Resolvable Multipath Delay

The periodicity of the transmitted PN places an upper bound on the maximum resolvable multipath delay, denoted  $\tau_{max}$ .

$$\tau_{max} = \frac{L}{f_c} \quad (46)$$

Multiplying  $\tau_{max}$  by the free space propagation velocity,  $c$ , yields the maximum resolvable path length  $d_{max}$ .

$$d_{max} = c \frac{L}{f_c} \quad (47)$$

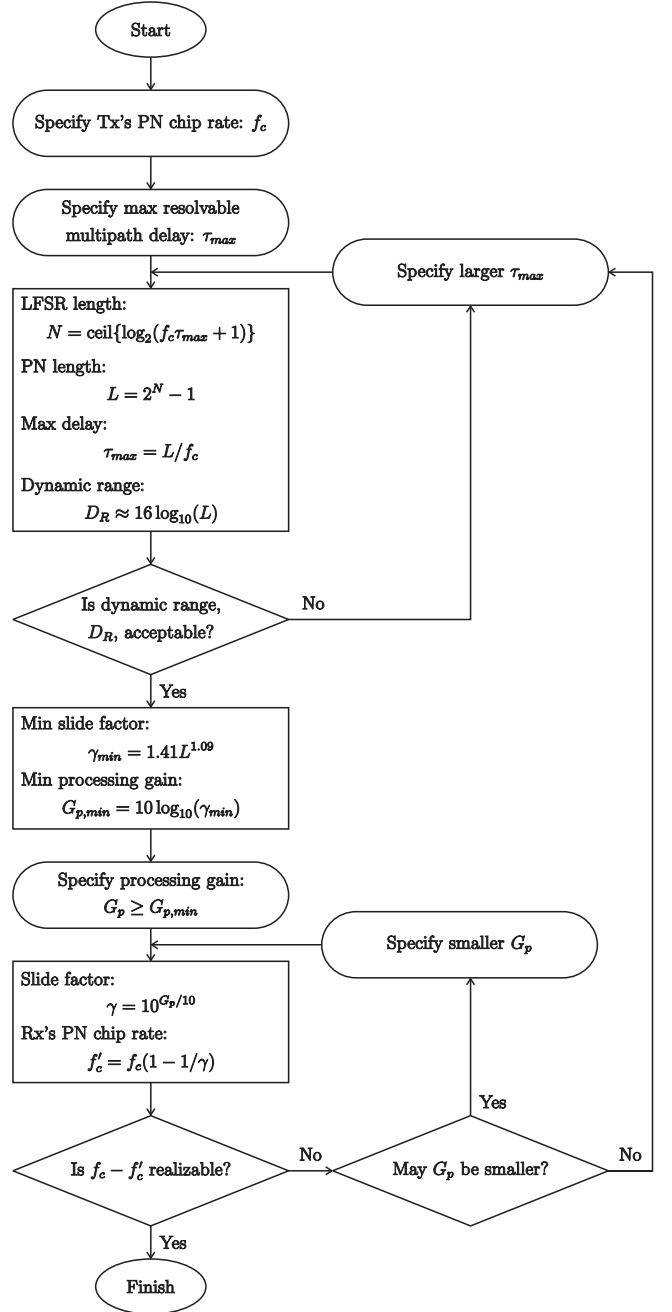


Fig. 9. Flowchart describing the design methodology for a sliding correlator channel sounder.

## VII. DESIGN METHODOLOGY

Re-examining Table I, we note that only  $f_{D,max}$  is adversely affected by increasing  $\gamma$ . This indicates that measuring a time-varying wireless channel requires special consideration to balance the tradeoffs in system performance for the specific scenario. However, for static channels, a logical design process follows from the equations in Table I. Figure 9 diagrams this design process. To specify  $f_c$ , recall that the chip rate is approximately equal to the baseband bandwidth of the transmitted signal.

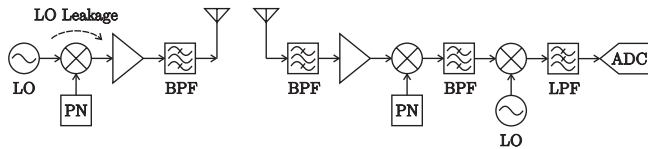


Fig. 10. A simplified diagram of the sliding correlator channel sounder. Poor LO-RF isolation allows a portion of the LO power to leak through to the RF port. This acts as a narrowband interferent at the receiver.

### VIII. PRACTICAL DESIGN CONSIDERATIONS

In Figure 9, the final decision block concerning the realizability of  $f_c - f'_c$  represents one of several practical considerations for system design. Depending on the quality factor of the reference oscillators and the specific choice of  $f_c$  and  $f'_c$ , minor phase variations between transmitter and receiver can cause major fluctuations in  $f_c - f'_c$ . This causes deviations in the slide factor that degrade the system's performance. Phase instability poses additional challenges for those seeking absolute delay and phase measurements. The preferred solution for achieving phase stability in channel measurements is to use rubidium or cesium-based atomic master oscillators, which offer extremely high phase stability but can be prohibitively expensive [17]. A more economical solution is to phase-lock the reference oscillators via a cable, but this hampers the mobility and utility of the system.

The channel sounder's performance will also be affected by the limitations and non-idealities of hardware. Amplifier bandwidth, noise figure, 1 dB compression point, mixer port isolation, and conversion losses will all degrade the theoretical system performance. Of the aforementioned design specifications, the most critical for the sliding correlator channel sounder is high mixer LO-RF isolation. Poor isolation allows a portion of the LO power to leak into the RF port of the mixer, as depicted in Figure 10. This acts as narrowband interference at the carrier frequency that essentially raises the receiver noise floor and degrades the dynamic range. The effects of LO leakage may be mitigated by increasing the slide factor to increase  $G_p$ , but this will adversely affect other aspects of the system as evidenced by Table I.

### IX. IMPLICATIONS OF TIME-VARYING CHANNELS

For time-varying channel measurements, it is important to recognize that the sliding correlator's time-dilated impulse response is *not* equivalent to a time-dilated copy of the channel's actual impulse response. To clarify this point, it is helpful to consider Figure 11, which presents the signal's spectrum at various stages within the sliding correlator channel sounder for both static and time-varying channels. As both Fig. 11 and Eq. (13) indicate, the transmitted signal's spectrum is composed of discrete spectral tones interspaced by  $f_c/L$ . Propagation through the wireless channel serves to modulate each of these spectral tones according to that frequency's Doppler spectrum. The sliding correlator then convolves the received spectrum with the receiver's PN spectrum to generate the time-dilated CIR. Fundamentally, the temporal dilation and thereby, the bandwidth compression of the sliding correlator arises because this convolution applies a frequency shift to each of the modulated tones that reduces the spacing

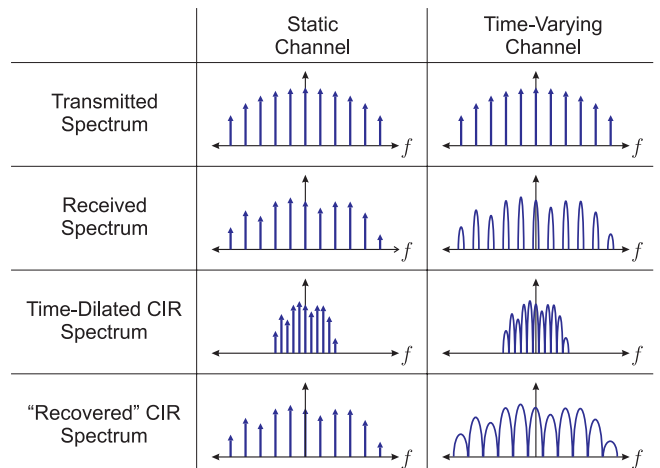


Fig. 11. The signal spectra at various points within the sliding correlator channel sounder indicate that only static channels permit recovery of the channel's true impulse response by temporally rescaling the sliding correlator's time-dilated CIR. Attempting to recover a time-varying channel's impulse response by similarly rescaling the time-dilated CIR will artificially broaden the observed Doppler spectra.

between tones' centers from  $f_c/L$  to  $(f_c - f'_c)/L$ . For the case of a static channel, we note that the channel's Doppler spectra are impulses centered at zero. Thereby, the received spectrum is discrete, and the sliding correlator's shifting of tones is equivalent to rescaling the spectrum. Thus, the static channel's impulse response may be recovered by temporally rescaling the sliding correlator's time-dilated CIR, as was shown in Eq. (41). For time-varying channels, however, the sliding correlator's frequency shifting cannot be interpreted as a frequency scaling because the transmitted tones have been spectrally broadened. As Fig. 11 indicates, temporally rescaling the sliding correlator's time-dilated CIR in attempts to recover the time-varying channel's true impulse response will artificially broaden the observed Doppler spectra. Instead, to accurately recover the time-varying channel's true impulse response, each of the modulated tones must be frequency shifted so as to restore the  $f_c/L$  spacing between the tones' centers and thereby, undo the sliding correlator's bandwidth compression.

Despite this additional overhead, we observe from Fig. 11 that provided the spectra of the modulated tones do not overlap in the time-dilated CIR's spectrum, the sliding correlator channel sounder unambiguously captures the channel's delay-Doppler characteristics. Note that this restriction is equivalent to requiring that the channel's maximum Doppler frequency be less than the system's Doppler resolution as given by Eq. (42) so as to prevent aliasing. It should be further noted that the additional post-processing needed to recover a time-varying channel's impulse response may be avoided in many measurement scenarios. For example, if one is interested in the underlying static component of a time-varying channel, provided that the time-varying component is an ergodic zero-mean process, the underlying static channel's impulse response may be found by appropriately time-averaging consecutive time-dilated CIRs and rescaling the result. If the time-varying channel is quasi-static such that its temporal coherence is significantly greater than the measurement period, the time-

dilated CIR may be treated analogously to the static channel case, because the impact of Doppler broadening due to temporal rescaling will be negligible. Finally, for those solely interested in a time-varying channel's Doppler characteristics, integrating consecutive periods of the time-dilated CIR will directly yield the time-varying channel provided that the channel is ergodic with respect to frequency [20].

## X. CONCLUSION

The sliding correlator channel sounder will continue its invaluable role in the investigation of current and future wireless channels. The versatility of the architecture makes it a cost-effective solution for any number of channel measurement scenarios characterized by large bandwidths, mobile transceivers, or even multiple antennas. The design methodology in Section VII describes a systematic approach to channel sounder design based upon a rigorous analysis of the sliding correlator. The derivation of a new minimum slide factor coupled with a modified expression for dynamic range provide realistic descriptions of the system's capabilities and enable researchers to design optimal sliding correlator channel sounders for high-fidelity measurements of next-generation wireless channels.

## REFERENCES

- [1] D. M. J. Devasiratham, "Time delay spread and signal level measurements of 850 MHz radio waves in building environments," *IEEE Trans. Antennas Propag.*, vol. 34, no. 11, pp. 1300–1305, Nov. 1986.
- [2] T. S. Rappaport, "Characterization of UHF multipath radio channels in factory buildings," *IEEE Trans. Antennas Propag.*, vol. 37, no. 8, pp. 1058–1069, Aug. 1989.
- [3] H. Xu, T. S. Rappaport, R. J. Boyle, and J. H. Schaffner, "Measurements and models for 38-GHz point-to-multipoint radiowave propagation," *IEEE J. Select. Areas Commun.*, vol. 18, no. 3, pp. 310–321, Mar. 2000.
- [4] C. R. Anderson and T. S. Rappaport, "In-building wideband partition loss measurements at 2.5 and 60 GHz," *IEEE Trans. Wireless Commun.*, vol. 3, no. 3, pp. 922–928, May 2004.
- [5] D. C. Cox, "Delay Doppler characteristics of multipath propagation at 910 MHz in a suburban mobile radio environment," *IEEE Trans. Antennas Propag.*, vol. 20, no. 5, pp. 625–635, Sept. 1972.
- [6] R. C. Dixon, *Spread Spectrum Systems with Commercial Applications*. John Wiley and Sons, Inc., 1994.
- [7] G. D. Durgin, V. Kukshya, and T. S. Rappaport, "Wideband measurements of angle and delay dispersion for outdoor and indoor peer-to-peer radio channels at 1920 MHz," *IEEE Trans. Antennas Propag.*, vol. 51, no. 1, pp. 936–944, May 2003.
- [8] T. Takeuchi and M. Tamura, "An ultra-wide band channel sounder for mobile communication systems," in *Proc. 12th IEEE International Symposium on Personal, Indoor and Mobile Radio Communications, 2001*, vol. 2, 2001, pp. E111–E115.
- [9] A. Durantini and D. Cassioli, "A multi-wall path loss model for indoor UWB propagation," in *Proc. IEEE Vehicular Technology Conference*, vol. 1, 2005, pp. 30–34.

- [10] S. Salous and V. Hinozroza, "Wideband indoor frequency agile channel sounder and measurements," *IEE Proc.-Microw. Antennas Propag.*, vol. 152, no. 6, pp. 573–580, Dec. 2005.
- [11] S. Salous, N. Nkiandrou, and N. F. Bajj, "Digital techniques for mobile radio chirp sounder," *IEE Proc.-Commun.*, vol. 145, no. 3, pp. 191–196, 1998.
- [12] W. G. Newhall, T. S. Rappaport, and D. G. Sweeney, "A spread spectrum sliding correlator system for propagation measurements," *RF Design*, pp. 40–54, Apr. 1996.
- [13] N. Benvenuto, "Distortion analysis on measuring the impulse response of a system using a crosscorrelation method," *AT&T Bell Lab. Techn. J.*, vol. 63, no. 10, pp. 2171–2192, Dec. 1984.
- [14] J. Talvitie and T. Poutanen, "Self-noise as a factor limiting the dynamic range in impulse response measurements using sliding correlation," in *Proc. IEEE International Symposium on Spread Spectrum Techniques and Applications '94*, July 1994, pp. 619–623.
- [15] G. Martin, "Wideband channel sounding dynamic range using a sliding correlator," in *Proc. VTC 2000-Spring Tokyo*, ser. VTC Conf. Proc., vol. 3, May 2000, pp. 2517–2521.
- [16] S. W. Golomb, *Shift Register Sequences*, revised ed. Laguna Hills, CA: Aegean Park Press, 1982.
- [17] C. Anderson, "Design and implementation of an ultrabroadband millimeter-wavelength vector sliding correlator channel sounder and in-building multipath measurements at 2.5 & 60 GHz," master's thesis, Virginia Tech, May 2002.
- [18] G. L. Turin, "Communication through noisy, random multipath channels," in *IRE Convention Record, 1956*, pp. 154–166.
- [19] P. C. Fannin, A. Molina, S. S. Swords, and P. J. Cullen, "Digital signal processing techniques applied to mobile radio channel sounding," in *Radar and Signal Processing, IEE Proceedings F*, vol. 8, no. 5, Oct. 1991, pp. 502–508.
- [20] G. Durgin, *Space-Time Wireless Channels*. Upper Saddle River, NJ: Prentice Hall Inc., 2003.



**Ryan J. Pirkel** received the B.S. and M.S. degrees in electrical engineering from the Georgia Institute of Technology in 2005 and 2007, respectively. He is currently pursuing a Ph.D. degree in electrical engineering and studying in situ measurement techniques for characterizing radio wave propagation mechanisms. His research interests are radio wave propagation, RF engineering, and analytical electromagnetics.



**Gregory D. Durgin** joined Georgia Tech's Department of Electrical and Computer Engineering as an assistant professor in 2003. His primary research areas are radio wave propagation, radiolocation, and applied electromagnetics. He received the BSEE (96), MSEE (98), and PhD (00) degrees from Virginia Polytechnic Institute and State University. In 2001 he was awarded a Japanese Society for the Promotion of Science (JSPS) Post-doctoral Fellowship and spent one year as a visiting researcher at Morinaga Laboratory in Osaka University. In 1998

he received the Stephen O. Rice prize (with coauthors Theodore S. Rappaport and Hao Xu) for best original journal article in the IEEE TRANSACTIONS ON COMMUNICATIONS. Prof. Durgin authored *Space-Time Wireless Channels*, the first textbook in the field of space-time channel modeling. He has won numerous teaching awards at Georgia Tech.